Coulomb Stress Evolution History as Implication on the Pattern of Strong Earthquakes along the Xianshuihe-Xiaojiang Fault System, China

Bing Yan[*1, 2], **Shinji Toda**[3], **Aiming Lin**[2]

1. *School of Earth Sciences and Engineering, Nanjing University, Nanjing* 210023, *China*
2. *Department of Geophysics, Graduate School of Science, Kyoto University, Kyoto* 606-8502, *Japan*
3. *International Research Institute of Disaster Science, Tohoku University, Sendai* 980-0845, *Japan*

Bing Yan: https://orcid.org/0000-0002-3489-7253

ABSTRACT: Coulomb stress accumulation and releasing history and its relationship with the occurrence of strong historical earthquakes could deepen our understanding of the occurrence pattern of strong earthquakes and hence its seismic potential in future. The sinistral strike-slip Xianshuihe-Xiaojiang fault zone (XXFS) is one of the most dangerous fault zones in China, extending 1 500-km-long from the central Tibetan Plateau to the Red River fault zone. There are 35 $M \geq 6.5$ historical earthquakes occurred since 1327, hence it is an ideal site for studying the Coulomb stress evolution history and its relationship with the occurrences of strong earthquakes. In this study, we evaluated the Coulomb stress change history along the XXFS by synthesizing fault geometry, GPS data and historical earthquakes. Coulomb stress change history also revealed different patterns of historical earthquakes on different segments of the XXFS, such as characteristic recurrence intervals along the Salaha-Moxi fault and super-cycles along the Xianshuihe fault. Based on the occurrence pattern of past historical earthquakes and current Coulomb stress field obtained in this study, we suggest positive ΔCFS and hence high seismic potential along the Salaha-Moxi fault and the Anninghe fault.
KEY WORDS: Tibetan Plateau, Xianshuihe-Xiaojiang fault system, Coulomb stress triggering theory, recurrence interval, seismic hazard.

0 INTRODUCTION

Knowledge of earthquake recurrence regularities is essential to understand potential future behavior and to estimate seismic hazard of an active fault (Stein et al., 2012; Nishenko and Buland, 1987; Schwartz and Coppersmith, 1984; Shimazaki and Nakata, 1980). Earthquake interaction model and stress-triggering theory of earthquakes have been generally applied since two decades ago to evaluate earthquake interactions (Toda and Stein, 2002; Harris, 1998; King et al., 1994). Major active strike-slip faults with high seismicity, such as the San Andreas fault, eastern California shear zone and North Anatolian fault, have provided many objects to examine the rationality of this theory (Toda et al., 2005; Lin and Stein, 2004; Stein et al., 1997). Stress changes deduced from completely revealed sequence of large earthquakes along the fault and adjacent faults have offered crucial quantitative restriction to the understanding of earthquake recurrences (e.g., Toda and Stein, 2002; Stein et al., 1997).

The 1 500-km-long Xianshuihe-Xiaojiang fault system

(XXFS) is one of the major strike-slip fault zones playing important roles in the tectonic evolution of the Tibetan Plateau (TP) (e.g., Wang and Burchfiel, 2000; Wang et al., 1998; England and Molnar, 1990). Both long-term and short-term slip rates in the order of ~10 mm/yr have been generally revealed both by geological investigations and geodetic observations (e.g., Yan and Lin, 2015; Zhang, 2013; Wang S F et al., 2009; Shen et al., 2005). A primary rupture history including 35 $M \geq 6.5$ historical earthquakes with strike-slip focal mechanisms during the past ~700 years has been sorted out based on historical documents and instrumental records (Wen et al., 2008; EDPDCEA, 1995; Allen et al., 1991). The problem with the historical records is that it is shorter in remote areas such as on the TP, and that the more ancient and remote are the events, the less are the records based on which rupture locations and magnitudes are estimated. Modern instrumental records have problems of shorter period and incompleteness as well. For example, the focal mechanism of the 1955.04.14 M 7.5 Zheduotang Earthquake had been solved whereas the magnitude could not be calculated based on poor instrumental records. That is the reason why a great deal of paleoseismologic investigations have focused on these historical earthquakes (e.g., Ren, 2013; Ren and Lin, 2010; Wen et al., 2003).

There are many modeling works of stress evolution along the XXFS and adjacent area (e.g., Shao et al., 2016; Qin et al.,

---

2014; Shan et al., 2013; He et al., 2011; Zhu and Wen, 2010). After the 2008 M_w 7.9 Wenchuan Earthquake, Shan et al. (2013) calculated the Coulomb stress evolution along the XXFS during the past 300 yr and revealed earthquake interaction between the XXFS and the Longmen Shan thrust belt. Coulomb stress evolution along the Xianshuihe fault zone (XshFZ, the abbreviation is in order to mark off from the Xiaojiang fault zone) over the past 200 yr has been also calculated by Shao et al. (2016) to estimate seismic hazard along the central XshFZ. Studies on the parkfield earthquake revealed that well understanding of recurrence model is inessential for highly efficient seismic hazard assessment (e.g., Toda and Stein, 2002). Whereas recurrence model diversification was not taken into consideration in the previous modeling works along the XXFS.

In this study, we carried out Coulomb stress change modeling, in combination with paleoearthquake investigations, to examine the rupture history during the past ~1 000 yr and its implication for the recurrence models along the XXFS, which suggests stress change history as reliable constraints on seismic hazard assessment as well as paleoseismological investigations.

1 TECTONIC SETTING

The XXFS extends from the central TP to the Yungui Plateau until Red River fault zone and varies in trend from WNW-ESE at northwestern end to S-N at southeastern end, having the geometry of an arc projecting northeastwards (Fig. 1). It is composed of 6 fault zones, which from northwest to southeast are the WNW-ESE-trending Ganzi-Yushu fault zone (GYFZ), the NW-SE-trending XshFZ, the AZFZ composed of the S-N-trending Anninghe fault (AF), the NW-SE-trending Zemuhe fault (ZF), the NNW-SSE-trending Daliangshan fault zone (DFZ) and the S-N-trending along the southeastern Xiaojiang fault zone (XjFZ) (Fig. 1b). The GYFZ steps leftward for 18 km to the XshFZ, then branches at the southeastern end of the XshFZ into the AZFZ and DFZ, which then join into the XjFZ to the south (Fig. 1b). The GYFZ, XshFZ and AZFZ are mainly developed with continuous single fault traces respectively, except for the echelon fault structures of the central XshFZ. The fault traces of the DFZ are disconnected and shows echelon pattern. The fault traces of the XjFZ are in divergence pattern southward, and composed of two major branches and several sub faults. GYFZ and XshFZ distribute on the TP where average elevation is ~4 000–5 000 m, and AZFZ, DFZ and XjFZ distribute mainly on the Yungui Plateau where average elevation is ~2 000–3 000 m a.s.l. (Fig. 1b).

Tectonically, the XXFS is mainly located in the Songpan-Ganzi Block to the northwest, which is a major tectonic element of the central and eastern TP, and the Yangtze Block to the southeast. The Songpan-Ganzi Block is mainly covered by thick sequence of Triassic flysch complex, known as the Songpan-Ganzi fold belt, and accompanied by outcrops of suture zone rocks and Early Cenozoic granite. The GYFZ is mainly developed along ophiolitic melanges that consists partly of the Jinsha suture zone and of the Ganzi-Litang suture zone. The XshFZ has mainly offset the strata of the Songpan-Ganzi fold belt and the Longmen Shan thrust belt, which mainly composed of Precambrian high-grade metamorphic rocks, and then extends into the Yangtze Block. Along the southeastern XXFS, the Yangtze Block is mainly covered by Precambrian high-grade metamorphic rocks and Paleozoic–Lower Mesozoic carbonate rocks known as South China fold and thrust belts.

The crustal thickness of the study area has been generally investigated by various methods such as seismic sounding, 3-D shear wave speed variation, teleseismic receiver functions and Bouguer gravity anomaly inversions (Jiang et al., 2012; Zhang et al., 2011; Wang C Y et al., 2009, 2007; Yao et al., 2008; Xu et al., 2007; Wang and Burchfiel, 2000). The eastern TP has been revealed to be 65–60 km thick (Zhang et al., 2011). The thickness reduced rapidly to 50–45 km along the AZFZ after across the margin of the TP (Yao et al., 2008). The crust is thinner further south, 45–40 km along the XjFZ.

Initiation time and total offset amount of the XXFS has been one of the essential issues related to the tectonic evolution models of the TP (e.g., Searle et al., 2011; Wang and Burchfiel, 2000; Avouac and Tapponnier, 1993; England and Molnar, 1990). Roger et al. (1995) investigated the Gongga granite along the central XshFZ and suggested that the emplacement and ductile deformation of the granite are synchronous. The U-Pb emplacement age of 12.8±1.4 Ma and the Rb-Sr minimum deformation age of 11.6±0.4 Ma together suggested sinistral faulting at the latest at 12 Ma along the XshFZ. New geochronological investigations of mica K/Ar and apatite fission-track ages suggested initiation time of the GYFZ and XjFZ as 13 and 5 Ma, respectively (Wang S F et al., 2009). On the basis of the deflection of topographic features including major rivers and margin of the TP, the offset of geological strata, and the Bouguer gravity anomaly data, Yan and Lin (2015) suggested total offset amount along the GYFZ-XFZ as ~60 km, and long-term slip rate of 4.6–12 mm/yr consequently.

2 DATA AND MODELING

The modeling is carried out in Coulomb 3.3, which is a simple tool that permits exploration of a key component of fault interaction by excluding complicated processes such as dynamic stresses, pore-fluid diffusion, and viscoelastic rebound. It offers the function to calculate static stress change in an elastic half-space with uniform isotropic elastic properties at any depth caused by fault slip including both coseismic slip and secular slip (Toda et al., 2011).

2.1 Crustal Structure and Faults Geometry

Along most strike-slip faults except for a few creeping ones globally, the Coulomb stress release is mainly resulted from coseismic ruptures of large earthquakes. For the interplate strike-slip faults that have cut through the whole crust such as the North Anatolian fault, stress increase is resulted from secular slip in the lower crust (e.g., Stein et al., 1997). For the intraplate strike-slip XXFS, we suppose that it is crustal scale and undergoes secular slip in the lower crust based the following evidences: (i) The GYFZ is developed along the suture zones formed during the India-Asia continental collision according to the geological map, although their relationships need further study. (ii) Crustal thickness variation along the XXFS based on Bouguer gravity anomaly suggested that the crust of the eastern Tibetan Plateau possibly has been offset for ~60 km (Yan and Lin, 2015; Jiang et al., 2012). (iii) 3D shear-wave speed model

suggested lateral variations in crustal structure and rheology, that is, the XshFZ marks the northern edge of a pronounced, laterally continuous zone with anomalously low velocity (Liu et al., 2014). (iv) Based on the integrative interpretation of travel-time data and amplitude information obtained from the deep seismic sounding experiment, it is inferred that the XjFZ has cut through the whole crust (Wang C Y et al., 2009). (v) GPS

observation revealed strain partitioning across the XXFS (e.g., Zhang et al., 2004).

Attitudes of the faults are essential to the modeling. Along the GYFZ, seismic moment tensor inversion after the 2010 M_w 6.9 Yushu Earthquake revealed dip angle of 83°SW (Liu et al., 2010). Along the XshFZ, P-waveform analysis of the 1973 M_w 7.4 and 1981 M_w 6.7 events revealed dip angle of 87°SW and
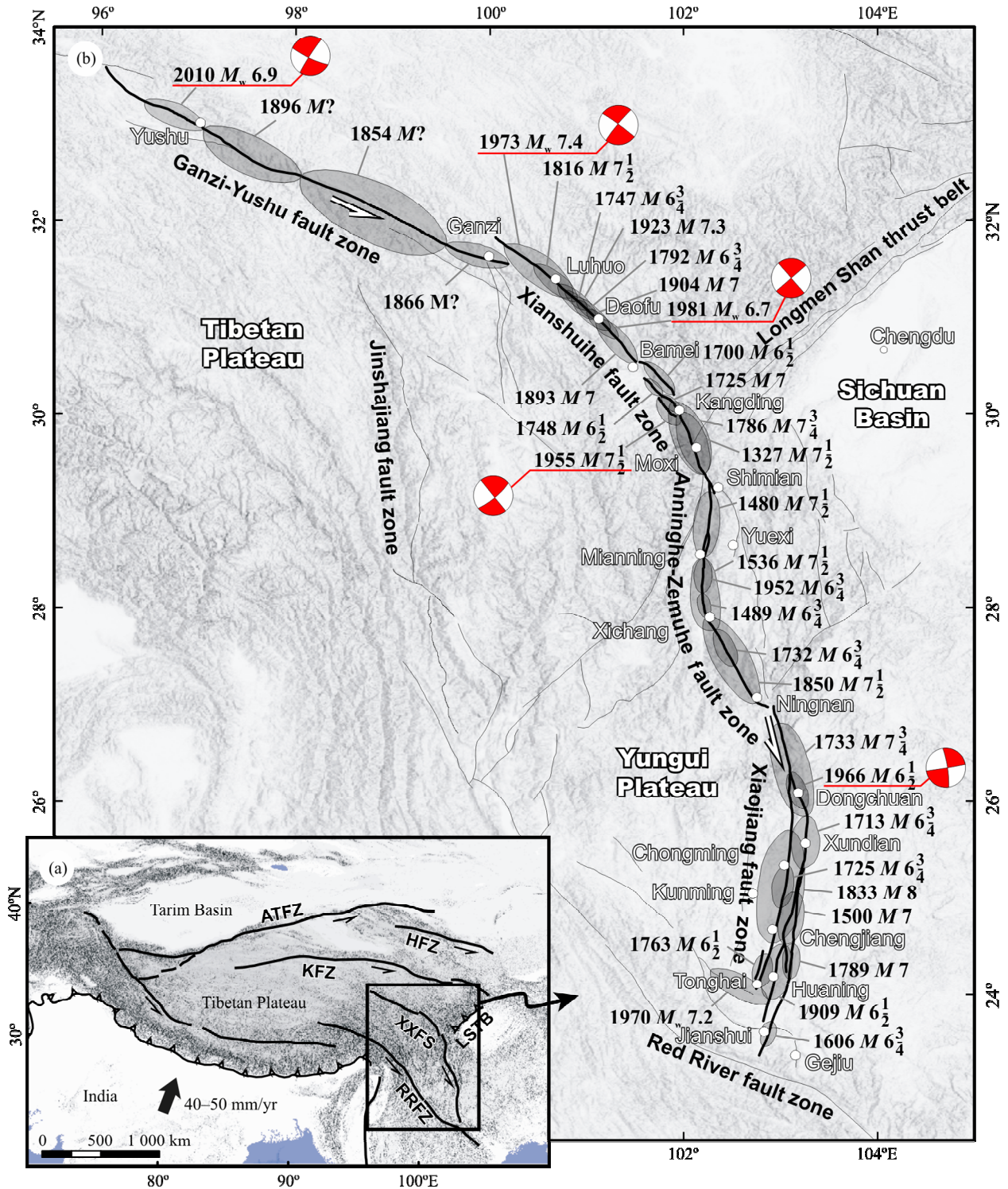

Figure 1. (a) Index map showing the tectonic setting of study area. (b) Main settlements along the XXFS, damage area of 35 historical earthquakes and focal mechanism solution of some model earthquakes. XXFS. Xianshuihe-Xiaojiang fault system; ATFZ. Altyn Tagh fault zone; HFZ. Hanyuan fault zone; KFZ. Kunlun fault zone; RRFZ. Red River fault zone; LSTB. Longmen Shan thrust belt.

90°, respectively (Zhou et al., 1983). The hypocenter depths of the above 3 events are all computed to be about 10 km (Liu et al., 2010; Zhou et al., 1983). Along the XjFZ, source depth and dip angle of the 1966 M 6.5 event are 5 km and 80°SW, respectively (Yan et al., 1980). Based on the above attitudes, we adopted simplified geometry of vertical co-seismic faults and secular faults in our modeling.

2.2   Historical Earthquakes

Many historical earthquakes and frequent modern earthquakes with extensive casualties and destruction have been recorded or reported along the XXFS (e.g., Wen et al., 2008; Allen et al., 1991; Tang et al., 1976; Heim, 1934). Historical literatures and modern publications are reviewed to determine rupture lengths of all the historical and modern earthquakes (Table 1; Fig. 1). Whereas the detail level and time period of earthquake records are not as good and long as densely populated plane area of China because of remote locations. Throughout history, settlements at the high plateau and mountain terrain have shown concentrated distribution along the fault traces, especially at fault valleys and pull-apart basins which are suitable for farming and grazing (Fig. 1b). As can be seen in the rupture history along the whole XXFS (Fig. 2), along the remotest GYFZ, only a few earthquakes at late 19th century with roughly speculated damage area and time are mentioned based on Tibetan civilian lore (Wen et al., 2003; Zhou et al., 1997). Whereas along the XshFZ, AZFZ and XjFZ, large historical earthquakes records with high reliability (recorded by adjacent settlements) cover a time period of ~300 years (Allen et al., 1991). Probable large earthquakes inferred from seisesthesia records of distant settlements can be traced back for ~700 years (Wen et al., 2008; EDPDCEA, 1995).

Parameters including rupture length and average displacements have been imported in our modeling. Wen et al. (2008, 2003) had reviewed the previous studies and provided

comprehensive parameters, to which data our modeling has mainly referred. Except for modern earthquakes such as the 2010 M_w 6.9 Yushu Earthquake (Wang and Mori, 2012) and a few historical ones that have been studied based on field investigations or seismic calculations (e.g., Ren, 2013), rupture length of most historical earthquakes have been estimated mainly according to historical documents. Intensity maps of all historical earthquakes have been firstly estimated based on historical documents. Probable ruptured areas as well as magnitudes are consequently speculated based on the intensity maps (e.g., Wen et al., 2008; EDPDCEA, 1995). Average displacements of all events have been derived from rupture lengths according to the empirical relationships among magnitude, rupture length and surface displacement for strike-slip fault as following (Wells and Coppersmith, 1994)

$$M_w=5.16+1.12 \cdot \lg \ SRL \qquad (1)$$

$$\lg AD= -6.32+0.09 \cdot M_w \qquad (2)$$

where M_w is moment magnitude, SRL is surface rupture length, AD is average displacement. The magnitude is the prerequisite to deduce rupture length and average offset, which is the basic parameters to calculate stress change caused by earthquakes. The magnitude and general rupture area of historical earthquakes could be estimated based on intensity map derived from historical documents, which only covers time period since 1327 in the study area. Therefore, we included historical earthquakes no earlier than 1327.

2.3   Holocene Sinistral Slip Rates along Each Segments

In addition to earthquakes, steady slip beneath the XXFS transfers stress to the seismogenic portion of the fault system. Before development of the Global Position System (GPS), the geological slip rate was mainly obtained by investigating offset terraces and alluvial fans as shown in Fig. 3 and described in
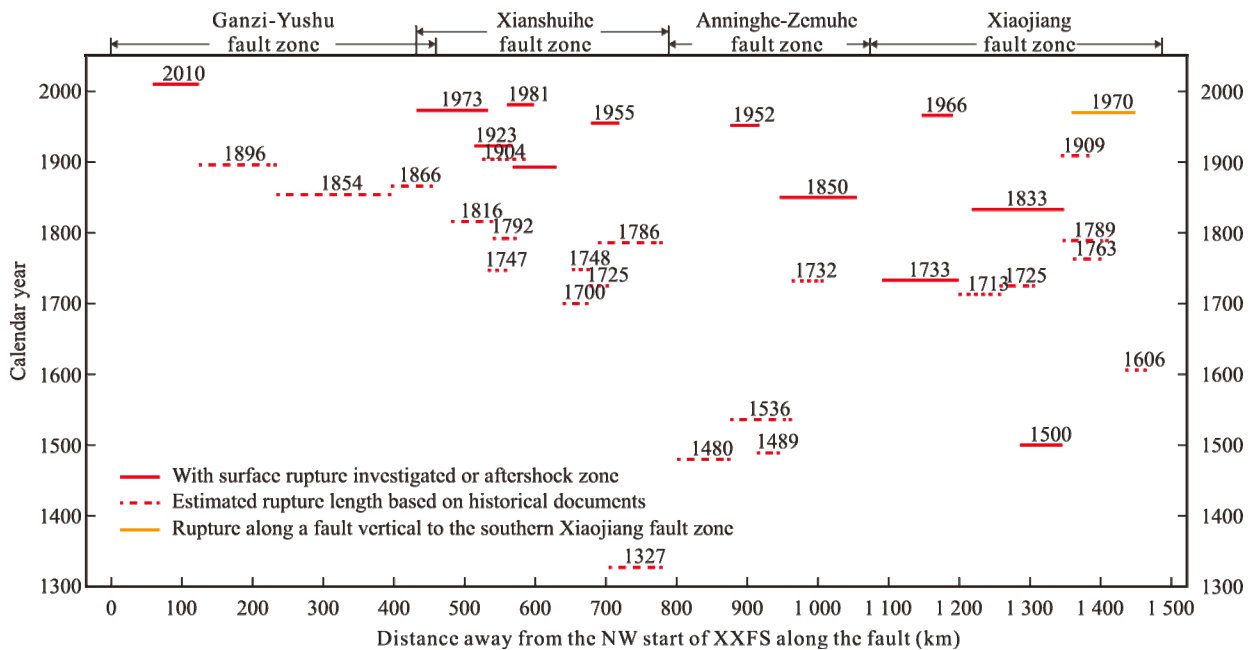

Figure 2. A spatial-temporal pattern of the rupture history of 35 $M \geq 6.5$ earthquakes along the XXFS.

Table 1 Historical earthquakes along the XXFS

Fault zone	Time (yy.mm.dd)	SRL (km)	M_s [a]	K M_w [b]	W & C M_w [c]	W & C Dave (m) [d]
Ganzi-Yushu	1854.--.--	160			7.6	3.5
Ganzi-Yushu	1866.--.--	65			7.2	1.4
Ganzi-Yushu	1896.03.--	110			7.4	2.4
Ganzi-Yushu	2010.04.14	60	7[e]	6.9	6.9[f]	0.8
Xianshuihe	1327.09.--	75	$\geq 7^1/_2$	7.4	7.3	1.6
Xianshuihe	1700.--.--	35	$>6^1/_2$	6.4	6.9	0.8
Xianshuihe	1725.08.01	27	7	6.8	6.8	0.6
Xianshuihe	1747.03.--	30	$6^3/_4$	6.7	6.8	0.7
Xianshuihe	1748.08.30	25	$6^1/_2$	6.4	6.7	0.5
Xianshuihe	1786.06.01	90	$7^3/_4$	7.7	7.3	2.0
Xianshuihe	1792.09.07	25	$6^3/_4$	6.7	6.7	0.5
Xianshuihe	1816.12.08	60	$7^1/_2$	7.4	7.2	1.3
Xianshuihe	1893.08.29	70	7	6.8	7.2	1.5
Xianshuihe	1904.08.30	55	7	6.8	7.1	1.2
Xianshuihe	1923.03.24	50	$7^1/_2$	7.4	7.1	1.1
Xianshuihe	1955.04.14	40	$7^1/_2$	7.4	7.0	0.9
Xianshuihe	1973.02.06	90	7.6[e]	7.5	7.4[f]	2.2
Xianshuihe	1981.01.24	45	6.9[e]	6.8	6.7[f]	0.5
Anninghe	1480.09.27	75	$7^1/_2$	7.4	7.3	1.6
Anninghe	1489.01.15	30	$6^3/_4$	6.7	6.8	0.7
Anninghe	1536.03.29	80	$7^1/_2$	7.4	7.3	1.7
Anninghe	1952.09.30	40	$6^3/_4$	6.7	7.0	0.9
Zemuhe	1732.01.29	45	$6^3/_4$	6.7	7.0	1.0
Zemuhe	1850.09.12	110	$7^1/_2$	7.4	7.4	2.4
Xiaojiang	1500.01.13	60	≥ 7	6.8	7.2	1.3
Xiaojiang	1606.11.30	30	$6^3/_4$	6.7	6.8	0.7
Xiaojiang	1713.02.26	60	$6^3/_4$	6.7	7.2	1.3
Xiaojiang	1725.01.08	50	$6^3/_4$	6.7	7.1	1.1
Xiaojiang	1733.08.02	110	$7^3/_4$	7.7	7.4	2.4
Xiaojiang	1763.12.30	40	$6^1/_2$	6.4	7.0	0.9
Xiaojiang	1789.06.07	60	7	6.8	7.2	1.3
Xiaojiang	1833.09.06	130	8	8.1	7.5	2.9
Xiaojiang	1909.05.11	40	$6^1/_2$	6.4	7.0	0.9
Xiaojiang	1966.02.05	45	6.5[e]	6.4	7.0	1.0
Xiaojiang	1970.01.05	85	7.7[e]	7.6	7.2[f]	1.4

[a]. Empirical surface wave magnitude from EDPDCEA (1999, 1995) derived from historical records about the event. [b]. Moment magnitude converted from surface wave magnitude based on the empirical relationships between surface wave magnitude and moment magnitude (Kanamori, 1983). [c]. Moment magnitude calculated based on the empirical relationships between magnitude and rupture length for strike-slip fault by Wells and Coppersmith (1994). [d]. Average diaplacment calculated based on the empirical relationships between magnitude and surface displacement for strike-slip fault by Wells and Coppersmith (1994). [e]. Surface wave magnitude from CENC (China Earthquake Networks Center) derived from seismometer records. [f]. Moment magnitude from USGS derived from seismometer records.

the following text. Dating techniques mainly include radiocarbon and thermoluminescence (TL) dating technique, except for a few cases using optically stimulated luminescence (OSL) dating technique. Along the GYFZ and the XshFZ on the Tibetan Plateau, slip rate was also estimated based on offset moraines formed during the last glaciation. The accuracy problem with dating technique and offset measuring might cause relative errors of slip rate even up to 50%. The corresponding error of recurrence intervals is thus far below expectation for the purpose of earthquake prediction. Thanks to decades of GPS observation on the TP, error of slip rate can be restricted within the limits of less than 10%–20% especially for those strike-slip faults of high slip rate (e.g., Zhang, 2013), providing much more reliable information on strain/stress accumulation rate (Fig. 3).

Along the GYFZ, Zhou et al. (1996) estimated Holocene slip rate to be 7±0.7 and 7.2±1.2 mm/yr along the eastern and central segments. Wen et al. (2003) obtained a larger Holocene slip rate of 12±2 mm/yr. Shi et al. (2016) estimated 8–11 mm/yr based partly on previous study and their own dating. The result obtained by Wang et al. (2013) based on GPS data observation from 1999 to 2007 is 6.6±1.5 mm/yr, which is comparable with the result of Zhou et al. (1996). Further northwest to the GYFZ is the active strike-slip Fenghuoshan fault zone (FFZ) with GPS slip rate of 6.1±1.9 mm/yr (Wang et al., 2013), which is also modeled in order to take the stress transformed from the secular slip beneath the FFZ to the GYFZ into account and eliminate boundary anomaly.

Along the northwestern segment of XshFZ, the only geological slip rate was estimated to be 15±5 mm/yr based on offset post-glacial terrace (Allen et al., 1991). Because of echelon pattern composed of three sub-faults along the central segment, the total geological slip rate is unequally divided along each sub-fault (Zhou et al., 2001a). Along the southeastern segment, Zhou et al. (2001b) estimated Holocene slip rate to be 6.0–9.9 mm/yr. The most recent Holocene slip rate along the southeastern segment was estimated to be ~8.5 mm/yr based on investigation of systematically offset channels and alluvial fans (Yan and Lin, 2017). GPS observation observed more accurate slip rates of ~9–10 mm/yr along the northwestern and southeastern segments respectively (Wang et al., 2013; Zhang, 2013; Shen et al., 2005).

GPS observation also obtained total slip rate of ~9–10 mm/yr across the split AZFZ and DFZ (Zhang, 2013). The problem is the distribution of the total slip rate along each segments. Along the AF and the ZF, Holocene slip rates were generally estimated to be ~5–6 mm/yr (Ren, 2014; Ran et al., 2008; He and Ikeda, 2007; Zhou et al., 2001b) and 27 to 5–9 mm/yr (He and Oguchi, 2008; He et al., 1999), respectively. Ren et al. (2010) estimated a much larger slip rate of ~10–12 mm/yr since ~44 ka ago along the ZF. Along the DFZ, an average slip rate of ~3 mm/yr was generally estimated (He et al., 2008; Zhou et al., 2003). Most of the geological slip rate shows comparable sum value to the GPS data.

The XjFZ is composed of two main branches and several sub faults. The slip rate is more complex. He and Oguchi (2008) estimated really large total slip rate of 14–22 mm/yr based on TL and radiocarbon dating of offset channels, which is much larger than the GPS slip rate of 7±2 mm/yr (Shen et al., 2005). Based on seismic moment and recurrence interval, Li et al. (2013) estimated slip rate varies between 1.6–10.1 mm/yr at the depth range of 3–12 km.

Except for left-lateral slip rates, shortening rates of <2 mm/yr across the GYFZ, XshFZ, AF and extension rates of <2 mm/yr across the ZF were also inferred based on GPS observation (Wang
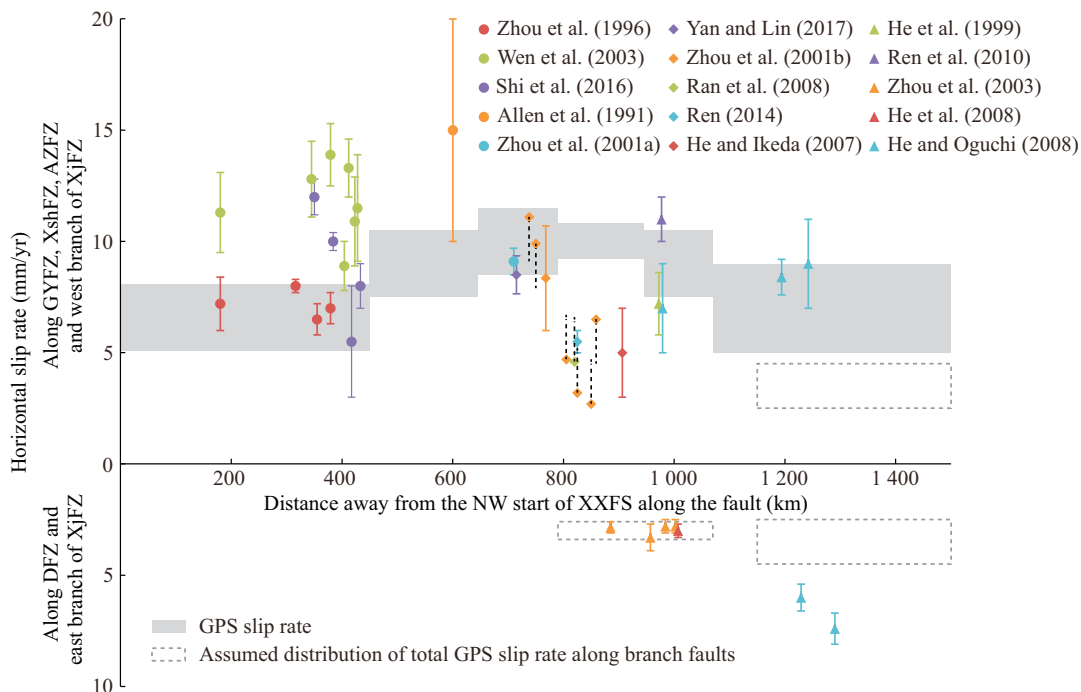

Figure 3. Geological and GPS slip rate of previous studies along the whole XXFS. Notice that the slip rate along the DFZ and east branch of XjFZ are displayed separately underneath. We assumed distribution of total GPS slip rate across the central and southeastern segments of the XXFS (AZFZ-DFZ and XjFZ) based on geological slip rate for the purpose of comparing geological and GPS slip rates.

et al., 2013; Zhang, 2013; Shen et al., 2005). We excluded these components in our modeling because of their low accuracy and much smaller proportion compared with the lateral slip rates.

2.4   Modeling and Results

Considering complexity of regional stress components along the XXFS (e.g., Gan et al., 2007), a uniaxial compression parameter is impractical, thus the stress is resolved on the fault plane (King et al., 1994). Since the hypocentral depths for the main shocks of the modern large earthquakes such as the 1973, 1981 and 2010 events are around 10 km, the modeling sample stress in the lower part of the seismogenic crust at a depth of 10 km. The friction coefficient on a fault is difficult to measure directly. A empirical value of μ' is as 0.4, which is similarly used for modeling the large cumulative slip fault zones such as the San Andreas fault (Toda et al., 2005; King et al., 1994).

We have mainly adopted the GPS slip rate to calculate stress accumulation transferred from the secular slip (Fig. 4a). GPS slip rates across AZFZ and DFZ were portioned according to the geological investigations described above. GPS data give 6 mm/yr along the Fenghuoshan fault zone (FFZ), 6.5 mm/yr along the GYFZ, 9–10 mm/yr along the XshFZ, 7 mm/yr along the AF, 6 mm/yr along the ZF, 3 along the DFZ and 7 mm/yr along the XjFZ. During a complete earthquake cycle in this model, coseismic slip would take place over 0–15 km and secular slip over 15–60 km (Fig. 4a). Coulomb stress on faults at a

depth of 10 km transferred from secular slip in this model is ~0.05–0.07 bar/yr along the GYFZ and ~0.09–0.1 bar/yr along the XshFZ, ~0.06–0.07 bar/yr along the AF and ZF, except for segments consisting of echelon faults (Fig. 4b). Because of the lack of historical earthquake records, stress evolution history was not calculated along the DFZ. The stress accumulation rate shows good proportion to the GPS slip rate, probably because of relatively smooth fault traces and our simplified geometry.

The southernmost XjFZ is composed of two major strands. Both of the strands have record of historical earthquakes. Because of unjustifiable proportion of the 7 mm/yr slip rate and lack of the geometry of seismogenic faults and deeper creeping faults, the transferred Coulomb stress is in a large variation range of 0.02–0.07 bar/yr while the deep creeping fault shifting between the threshold locations constrained by two major strands (cases 1 and 2 in Fig. 5). A compromising location (case 3) has been adopted finally based on consideration of reasonable stress change history on both branches (Fig. 5). The compromising location showing proximity to the western branch is consistent with the result of deep seismic sounding study of Wang C Y et al. (2009).

In order to model the accumulation and release of Coulomb stress along time, the Coulomb failure function is assumed to start from 1000 AD. The results are represented at the form of color gradient chart (Figs. 6 and 7a) and Coulomb stress evolution along time at selected locations (Figs. 7 and 8).
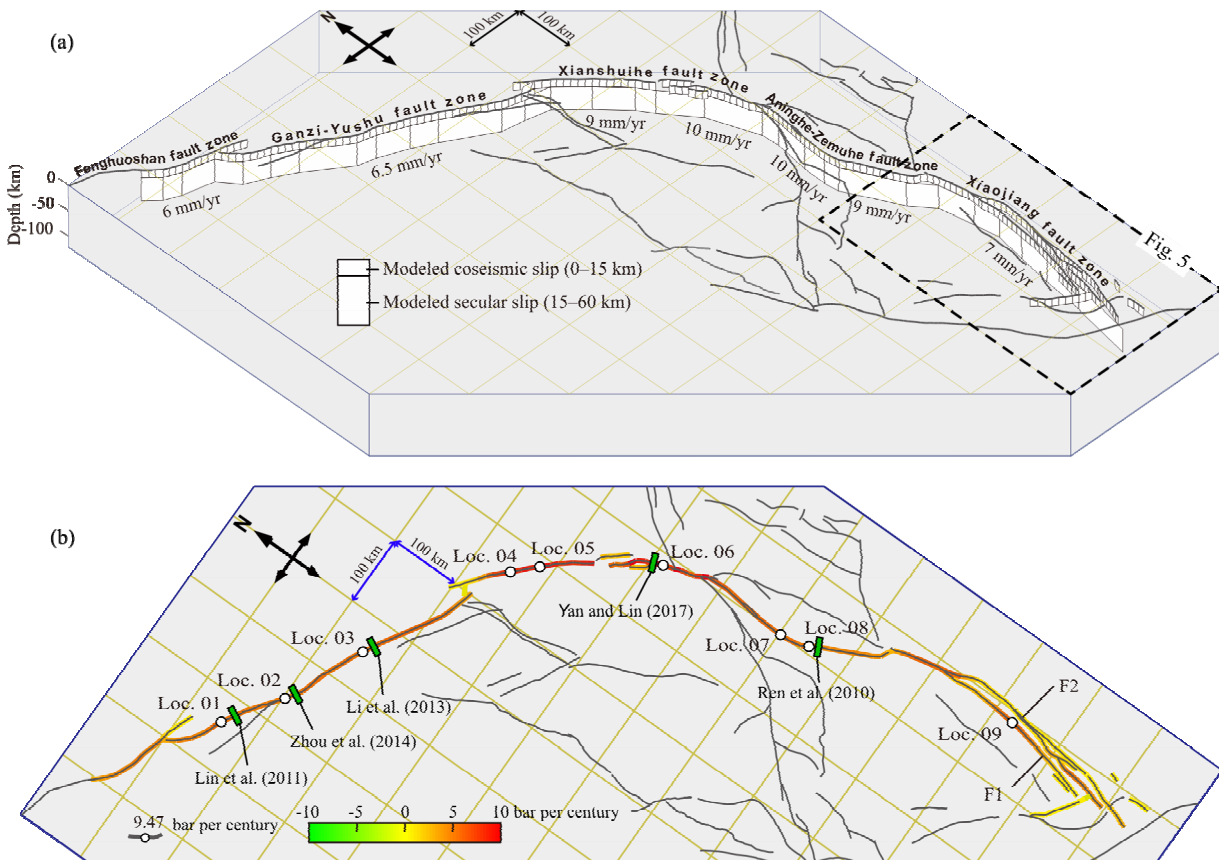

Figure 4. (a) Secular slip model used to calculate the loading of the XXFS. Steady deep slip below 15 km, as inferred from GPS observations (Wang et al., 2013; Zhang, 2013; Shen et al., 2005), transfers stress to the seismogenic portion of the fault. (b) The secular stress rate is resolved on the fault at the indicated points at a depth of 10 km. Locations have been selected to display stress change history in Figs. 7 and 8. Locations of previous paleoearthquake investigations have also been signed.
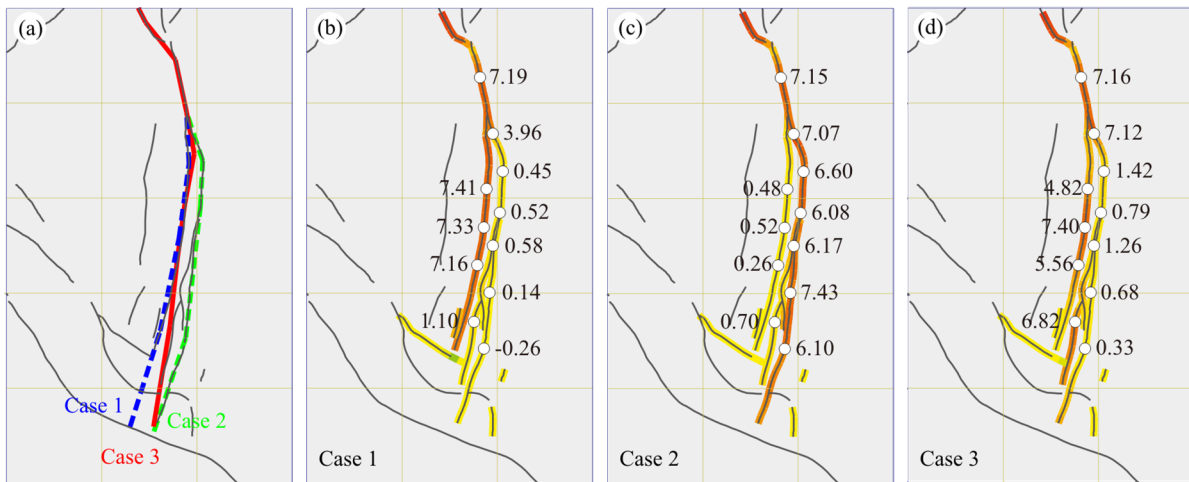
Figure 5. (a) Three cases of secular slip faults used to calculate the loading of the XjFZ. (b)–(d) The secular stress rate resolved on the fault at the indicated points at a depth of 10 km.

3 DISCUSSION

3.1 Implication to Recurrence Interval along the XXFS

Well understanding of recurrence model is essential for the successful probability calculation on the 2004 Parkfield Earthquake by Toda and Stein (2002). On the Tibetan Plateau, however, except for recurrence model along the eastern Haiyuan fault zone revealed by LiDAR investigation (Ren et al., 2015), recurrence models along most strike-slip faults such as the XXFS are still to be solved.

Stress changes history along the XXFS based on historical earthquakes displays great equilibrium (Fig. 6) because of integrity problem of historically recorded earthquakes along different segments. Along the GYFZ especially, the lack of historical earthquakes prior to 1850s has resulted in excess stress accumulation (Fig. 6). The Coulomb stress released by the 2010 M_w 6.9 Yushu Earthquake (~11 bar) along the northwest GYFZ is far from sufficient as compared to the accumulated during the past millennium (~65 bar) (Fig. 7b). Considering a similar magnitude earthquake with interval of ~600 yr as suggested by Lin et al. (2011), the rate of stress accumulation seems still faster than that of release. Along the southeastern GYFZ, the 1854 earthquake, magnitude of which is estimated from the preliminarily inferred surface rupture (Table 1), seems released most of the Coulomb stress (~48 bar) transferred from the secular faults during the past 900 yr (~60 bar) (Fig. 7d). The magnitude of an event with 160-km-long surface rupture is about M 7.5 and should be felt over an area with radius of >900 km (EDPDCEA, 1995). Whereas no historical shaking records on this event has been disclosure at surrounding settlements such as Luhuo, Daofu, Kangding or Chengdu, etc., this might indicate smaller magnitude of the 1854 event.

As complement to historical records, paleoearthquake investigations carried out along the fault system has primarily suggested a general range of recurrence interval varying between 300–700 yr along part of the XXFS. An ideal stress change history of the GYFZ based on paleoearthquake studies and stress release discussed above has thus been modeled (Fig. 7a). Except for the 1738 event, a shorter interval of 300 yr along the Yushu segment has been adopted. The 160-km-long

rupture of the 1854 event has been divided into two segments both with recurrence interval of ~500 yr. The ideal stress change history result, based on characteristic recurrence model and in great need of confirmation by further investigation, suggested general recurrence interval of ~300–500 yr and rupture length of shorter than ~100 km along the GYFZ (Fig. 7). Similar interval of ~370–460 yr has been revealed along the southeastern XFZ by trench investigation of Yan and Lin (2017) and shows consistency with stress change history (Fig. 8c).

Split of the sum slip rates has occurred along the central and southeastern XXFS, which might result in lower stress accumulation rate and longer interval. Along the AF, the stress change shows coincidence with the historical earthquakes with an interval of ~400 yr (Fig. 8d). Along the ZF, the trench investigation of Ren et al. (2010) suggested that a historical earthquake at 814AD prior to the 1536 event, with an interval of ~700 yr (Fig. 8e). Whereas it should be noted that the slip model might not be the characteristic along the AZFZ. Along the western branch of XjFZ, the 1833 event has released stress accumulated for ~800–1 000 yr, expecting much longer interval compared with other segments of the XXFS (Fig. 8f).

3.2 Implication to Earthquake Models and Seismic Hazard Assessment

A fundamental rule of a fully uncovered rupture history is the conservation of stress between accumulation and relief (Youngs and Coppersmith, 1985; Anderson and Luco, 1983; Wallace, 1970; Brune, 1968). The principle is generally followed by previous earthquake models, among which the characteristic earthquake model is ideal balanced-budget between stress accumulation and relief (Wesnousky, 1994; Bakun and Lindh, 1985; Shimazaki and Nakata, 1980). Actually there are conservative tendencies of global paleoearthquake investigations along preliminarily studied active faults to assume earthquake recurrence models as characteristic ones (e.g., Sieh, 1996; Wesnousky, 1994). In the above section, we also adopted characteristic model to discuss the recurrence interval along the XXFS.

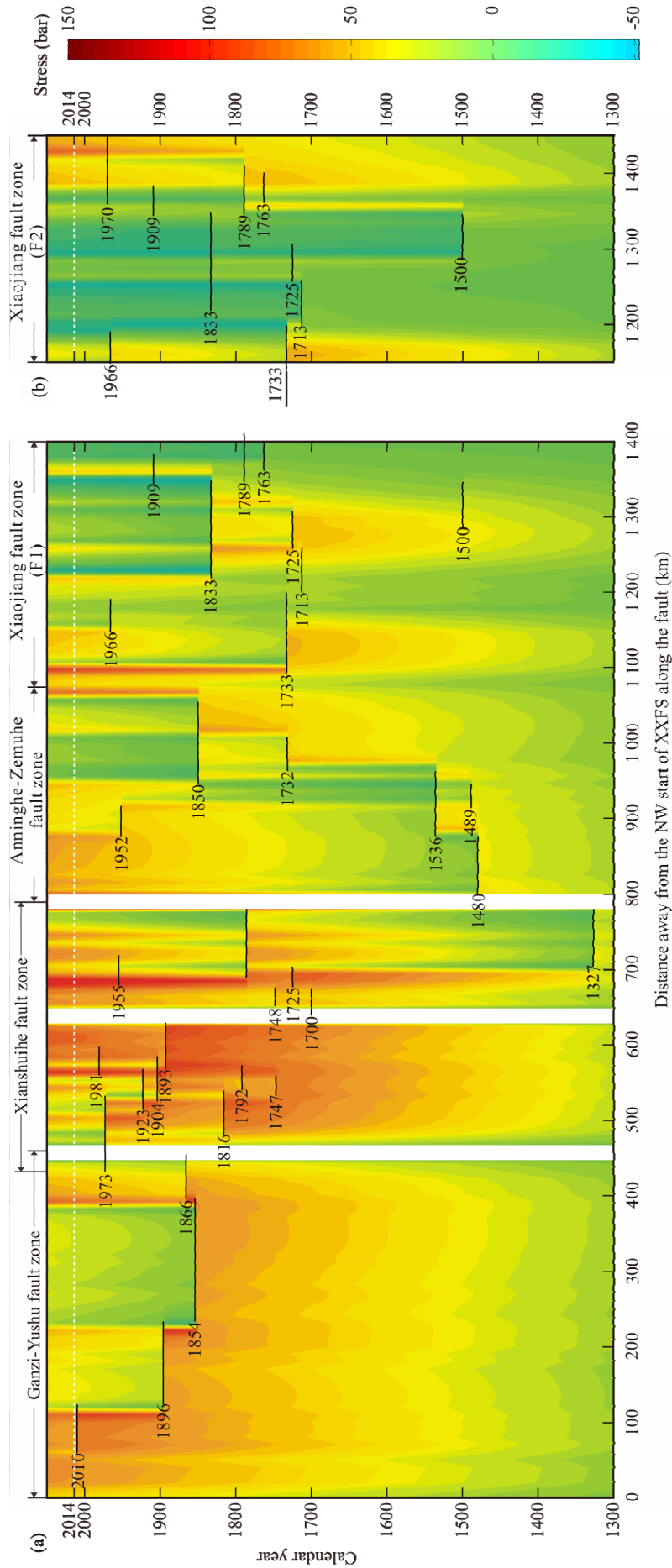Irregular patterns of earthquake recurrence such as clustered earthquakes have been concluded by geologists and

Figure 6. Raster showing stress change history along the XXFS. Along the XjFZ where there are two parallel strands, fault F1 is selected to display (see Fig. 4b for location). Notice the three white columns where main branches of the XXFS step to another.
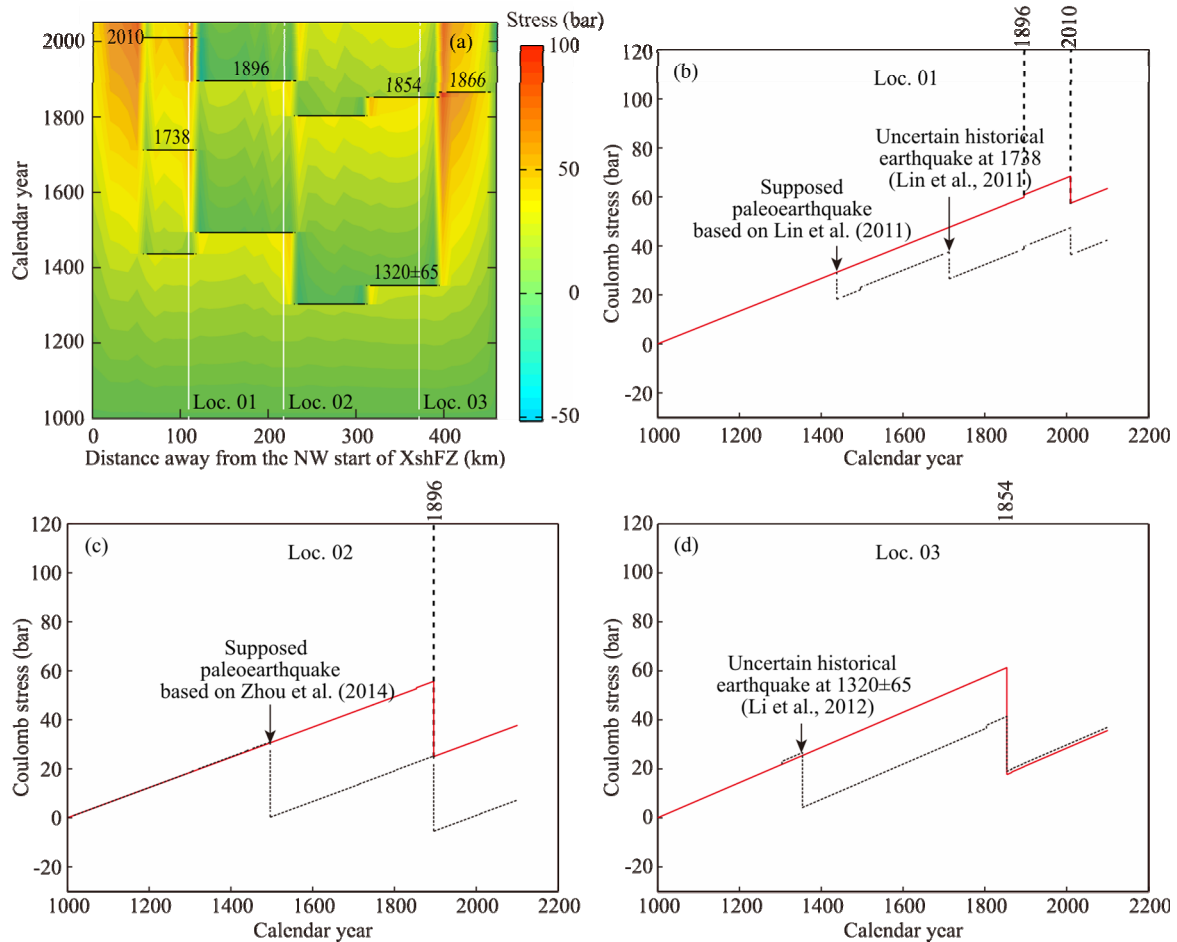
Figure 7. (a) Raster showing supposed stress change history along the GYFZ based on paleoearthquake investigations. Dashed lines are historical earthquakes. Dotted lines are supposed paleoearthquakes based on previous studies. (b)–(d) Coulomb stress accumulation and release at selected locations (see Fig. 4b and 7a for locations). Dashed lines are stress change history involving in supposed paleoearthquakes.

seismologists based on examination of ancient and modern patterns of large earthquakes (Grant and Sieh, 1994; Sieh et al., 1989; Thatcher, 1989; Matsuda et al., 1978). Most recent paleoseismic investigation combining quantitative constrains such as stress or strain change history have more precisely revealed the clustered pattern of recurrence interval (e.g., Schlagenhauf et al., 2011). The conception of earthquake supercycle has been proposed to explained the situation in which overlying and underlying blocks have been locked together, and strains continue to accumulate to a relatively high level and then released in the form of clustered earthquakes (e.g., Sieh et al., 2008). The northwest segment of XshFZ has experienced frequent rupture history, including four events with well-understood rupture lengths (1893, 1923, 1973, 1981; Figs. 2 and 6), suggesting recurrence interval obviously uncharacteristic. 50–100 bars stress is released during the last seismic cycle (Figs. 6, 8a, and 8b).

The central AZFZ is also characterized by clustering of earthquakes. Three historical earthquakes along the AF had caused obvious stress loading before the 1732 and 1850 events along the ZF (Figs. 6 and 8e). So it is the alternation before the 1952 event. Besides, trench investigation by Ren et al. (2010) suggested an historical earthquake at 814AD along the ZF. These historical earthquakes showed evidence of supercycles

and continuous migration between AF and ZF based on stress transferring. Besides, the stress along the AF seemed not sufficiently released after the 1952 event (Fig. 6).

Along the Selaha fault of the southeastern XshFZ, both historical records and paleoseismologic investigation suggested characteristic recurrence model. It has been ~230 yr since the 1786 event, which is shorter than the recurrence interval of ~370–460 yr. Whereas the most recent 1955 earthquake occurred along the branch Zheduotang fault has caused stress increase along the Selaha fault (Fig. 8c). Beside, the 2008 M_w 7.9 Wenchuan Earthquake also caused 0.2–0.5 bars closer to Coulomb failure (Toda et al., 2008). Current static stress along the Selaha fault seems have approximately reached to the level when the 1327 M 7.5 and 1786 M 7.75 earthquakes were triggered. Shao et al. (2016) calculated Coulomb stress evolution over the past 200 years along the GYFZ and also suggested high seismicity along the Selaha fault. A latest M_w 5.9 (M_s 6.3) earthquake with aftershocks has occurred on Nov. 22, 2014 along the northern Selaha fault where the 1725.08.01 M 7 historical earthquake is recorded.

4 CONCLUSION

Based on the modeling of Coulomb stress change on the seismogenic fault planes, we concluded that: Modeling of
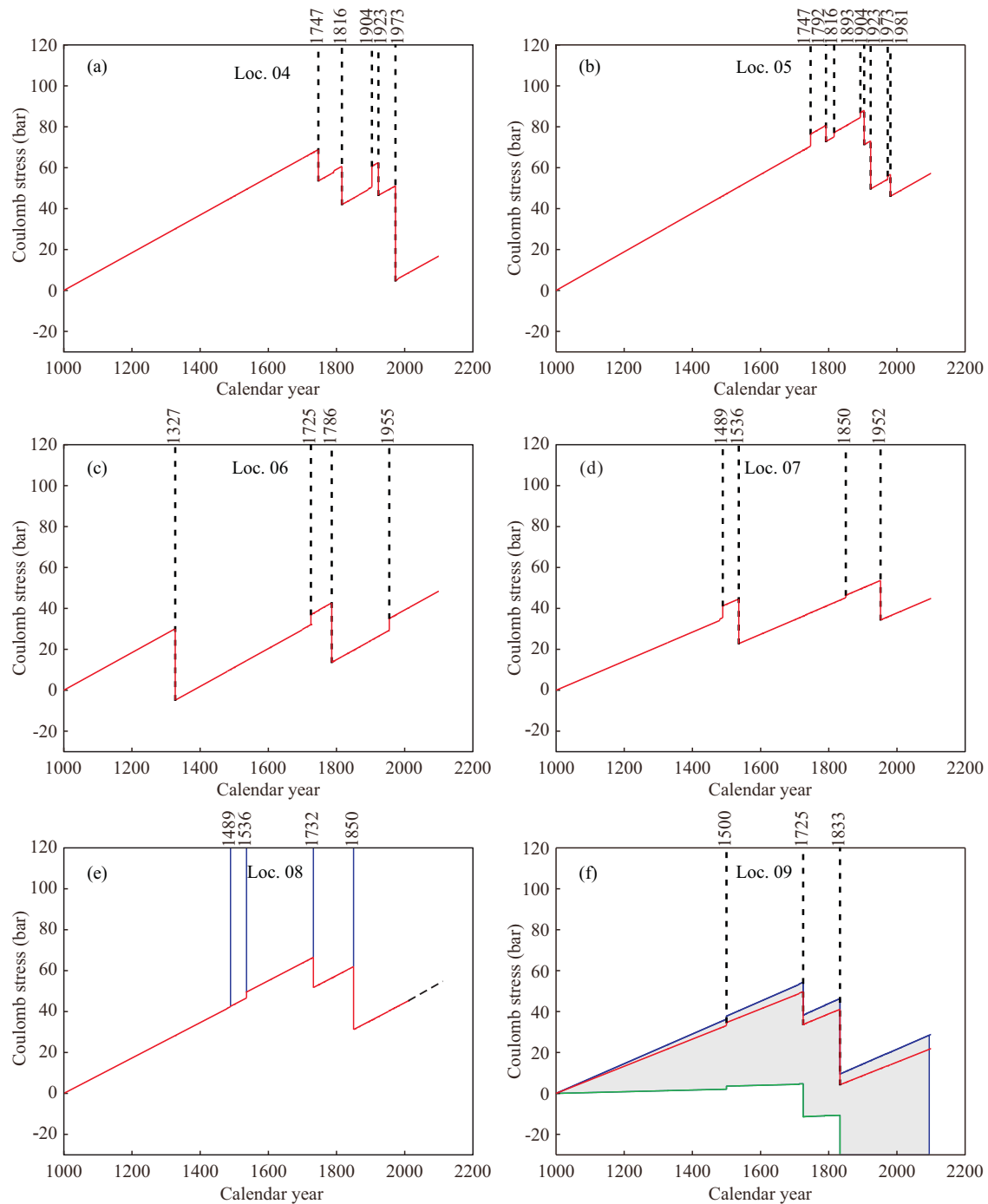
Figure 8. Coulomb stress accumulation and release at selected locations along the northwest XXFS (see Fig. 4b for locations). Notice that the result at loc. 09 (red line) has been compromised based on Fig. 5.

Coulomb stress change offers efficient quantitative methods to examine recurrence intervals revealed by paleoseismic investigation. The XXFS showed heterogeneous earthquake models along different segments. Characteristic recurrence interval suggested by Coulomb stress change history showed consistency with paleoearthquake investigations along the GYFZ and the southeastern XshFZ. Whereas the northeastern XshFZ and the central AZFZ showed evidence of supercycles. Earthquake occurred on adjacent faults had also caused stress accumulation closer to Coulomb failure along the southeastern XshFZ and the ZF. The Coulomb stress accumulated along the southeastern

XshFZ has approximately reached to the level when the most recent two large earthquakes were triggered.

ACKNOWLEDGMENTS

REFERENCES CITED

Allen, C. R., Luo, Z., Qian, H., et al., 1991. Field Study of a Highly Active Fault Zone: The Xianshuihe Fault of Southwestern China. *Geological Society of America Bulletin*, 103(9): 1178–1199

Anderson, J. G., Luco, J. E., 1983. Consequences of Slip Rate Constraints on Earthquake Occurrence Relations. *Bulletin of the Seismological Society of America*, 73(2): 471–496

Avouac, J. P., Tapponnier, P., 1993. Kinematic Model of Active Deformation in Central Asia. *Geophysical Research Letters*, 20(10): 895–898. https://doi.org/10.1029/93gl00128

Bakun, W. H., Lindh, A. G., 1985. The Parkfield, California, Earthquake Prediction Experiment. *Science*, 229(4714): 619–624. https://doi.org/10.1126/science.229.4714.619

Brune, J. N., 1968. Seismic Moment, Seismicity, and Rate of Slip along Major Fault Zones. *Journal of Geophysical Research*, 73(2): 777–784. https://doi.org/10.1029/jb073i002p00777

Earthquake Disaster Prevention Department of China Earthquake Administration (EDPDCEA), 1995. Catalogue of Chinese Historical Strong Earthquakes (23rd Century BC-AD 1911). Seismological Press, Beijing. 514 (in Chinese)

Earthquake Disaster Prevention Department of China Earthquake Administration (EDPDCEA), 1999. Catalogue of Chinese Modern Earthquake (1912 AD-1990 AD $M_s \geq$ 4.7). China Science and Technology Press, Beijing. 637 (in Chinese)

England, P., Molnar, P., 1990. Right-Lateral Shear and Rotation as the Explanation for Strike-Slip Faulting in Eastern Tibet. *Nature*, 344(6262): 140–142. https://doi.org/10.1038/344140a0

Gan, W. J., Zhang, P. Z., Shen, Z. K., et al., 2007. Present-Day Crustal Motion within the Tibetan Plateau Inferred from GPS Measurements. *Journal of Geophysical Research*, 112(B8): B08416. https://doi.org/10.1029/2005jb004120

Grant, L. B., Sieh, K., 1994. Paleoseismic Evidence of Clustered Earthquakes on the San Andreas Fault in the Carrizo Plain, California. *Journal of Geophysical Research*, 99(B4): 6819–6841. https://doi.org/10.1029/94jb00125

Harris, R. A., 1998. Introduction to Special Section: Stress Triggers, Stress Shadows, and Implications for Seismic Hazard. *Journal of Geophysical Research*: *Solid Earth*, 103(B10): 24347–24358. https://doi.org/10.1029/98jb01576

He, H. L., Ikeda, Y., 2007. Faulting on the Anninghe Fault Zone, Southwest China in Late Quaternary and Its Movement Model. *Acta Seismologica Sinica*, 20(5): 571–583. https://doi.org/10.1007/s11589-007-0571-4

He, H. L., Ikeda, Y., He, Y. L., et al., 2008. Newly-Generated Daliangshan Fault Zone—Shortcutting on the Central Section of Xianshuihe-Xiaojiang Fault System. *Science in China Series D*: *Earth Sciences*, 51(9): 1248–1258. https://doi.org/10.1007/s11430-008-0094-4

He, H. L., Oguchi, T., 2008. Late Quaternary Activity of the Zemuhe and Xiaojiang Faults in Southwest China from Geomorphological Mapping. *Geomorphology*, 96(1/2): 62–85. https://doi.org/10.1016/j.geomorph.2007.07.009

He, H. L., Song, F. M., Li, C. Y., 1999. Topographic Survey of Micro Faulted Landform and Estimation of Strike Slip Rate for the Zemuhe Fault, Sichuan Province. *Seismology and Geology*, 21(4): 361–369 (in Chinese with English Abstract)

He, J. K., Xia, W. H., Lu, S. J., et al., 2011. Three-Dimensional Finite Element Modeling of Stress Evolution around the Xiaojiang Fault System in the Southeastern Tibetan Plateau during the Past ~500 Years. *Tectonophysics*, 507(1/2/3/4): 70–85. https://doi.org/10.1016/j.tecto.2011.05.009

Heim, A., 1934. Earthquake Region of Taofu. *Geological Society of America Bulletin*, 45(6): 1035–1050. https://doi.org/10.1130/gsab-45-1035

Jiang, W. L., Zhang, J. F., Tian, T., et al., 2012. Crustal Structure of Chuan-Dian Region Derived from Gravity Data and Its Tectonic Implications. *Physics of the Earth and Planetary Interiors*, 212/213: 76–87. https://doi.org/10.1016/j.pepi.2012.07.001

Kanamori, H., 1983. Magnitude Scale and Quantification of Earthquakes. *Tectonophysics*, 93(3/4): 185–199. https://doi.org/10.1016/0040-1951(83)90273-1

King, G. C. P., Stein, R. S., Lin, J., 1994. Static Stress Changes and the Triggering of Earthquakes. *Bulletin of the Seismological Society of America*, 84(3): 935–953

Li, A., Shi, F., Yang, X. P., et al., 2012. Recurrence of Paleoearthquakes on the Southeastern Segment of the Ganzi-Yushu Fault, Central Tibetan Plateau. *Science China Earth Sciences*, 56(2): 165–172. https://doi.org/10.1007/s11430-012-4540-y

Li, L., Chen, Q. F., Niu, F. L., et al., 2013. Estimates of Deep Slip Rate along the Xiaojiang Fault with Repeating Microearthquake Data. *Chinese Journal of Geophysics*, 56(10): 3373–3384 (in Chinese with English Abstract)

Lin, A., Jia, D., Rao, G., et al., 2011. Recurrent Morphogenic Earthquakes in the Past Millennium along the Strike-Slip Yushu Fault, Central Tibetan Plateau. *Bulletin of the Seismological Society of America*, 101(6): 2755–2764. https://doi.org/10.1785/0120100274

Lin, J., Stein, R. S., 2004. Stress Triggering in Thrust and Subduction Earthquakes and Stress Interaction between the Southern San Andreas and nearby Thrust and Strike-Slip Faults. *Journal of Geophysical Research*: *Solid Earth*, 109(B2): B02303. https://doi.org/10.1029/2003jb002607

Liu, C., Xu, L., Chen, Y., 2010. IGP-CEA Moment Tensor Solution. [2018-3-8]. http://www.csi.ac.cn/manage/html/4028861611c5c2ba0111c5c558b00001/_content/10_04/17/1271488288058.html

Liu, Q. Y., van der Hilst, R. D., Li, Y., et al., 2014. Eastward Expansion of the Tibetan Plateau by Crustal Flow and Strain Partitioning across Faults. *Nature Geoscience*, 7(5): 361–365. https://doi.org/10.1038/ngeo2130

Matsuda, T., Ota, Y., Ando, M., et al., 1978. Fault Mechanism and Recurrence Time of Major Earthquakes in Southern Kanto District, Japan, as Deduced from Coastal Terrace Data. *Geological Society of America Bulletin*, 89(11): 1610–1618. https://doi.org/10.1130/0016-7606(1978)89<1610:fmarto>2.0.co;2

Nishenko, S. P., Buland, R., 1987. A Generic Recurrence Interval Distribution for Earthquake Forecasting. *Geological Society of America Bulletin*, 77(4): 1382–1399

Qin, X. H., Tan, C. X., Chen, Q. C., et al., 2014. Crustal Stress State and Seismic Hazard along Southwest Segment of the Longmenshan Thrust Belt after Wenchuan Earthquake. *Journal of Earth Science*, 25(4): 676–688. https://doi.org/10.1007/s12583-014-0457-z

Ran, Y., Cheng, J., Gong, H., et al., 2008. Late Quaternary Geomorphic Deformation and Displacement Rates of the Anninghe Fault around Zimakua. *Seismology and Geology*, 30(1): 86–98 (in Chinese with English Abstract)

Ren, Z. K., 2013. Geometry and Deformation Features of the most Recent Co-Seismic Surface Ruptures along the Xiaojiang Fault and Its Tectonic Implications for the Tibetan Plateau. *Journal of Asian Earth Sciences*, 77: 21–30. https://doi.org/10.1016/j.jseaes.2013.08.016

Ren, Z. K., 2014. Late Quaternary Deformation Features along the Anninghe Fault on the Eastern Margin of the Tibetan Plateau. *Journal of Asian Earth Sciences*, 85: 53–65. https://doi.org/10.1016/j.jseaes.2014.01.025

Ren, Z. K., Lin, A. M., 2010. Deformation Characteristics of Co-Seismic Surface Ruptures Produced by the 1850 *M* 7.5 Xichang Earthquake on

the Eastern Margin of the Tibetan Plateau. *Journal of Asian Earth Sciences*, 38(1/2): 1–13. https://doi.org/10.1016/j.jseaes.2009.12.008

Ren, Z. K., Lin, A. M., Rao, G., 2010. Late Pleistocene–Holocene Activity of the Zemuhe Fault on the Southeastern Margin of the Tibetan Plateau. *Tectonophysics*, 495(3/4): 324–336. https://doi.org/10.1016/j.tecto.2010.09.039

Ren, Z. K., Zhang, Z. Q., Chen, T., et al., 2015. Clustering of Offsets on the Haiyuan Fault and their Relationship to Paleoearthquakes. *Geological Society of America Bulletin*, 128(1/2): 3–18. https://doi.org/10.1130/b31155.1

Roger, F., Calassou, S., Lancelot, J., et al., 1995. Miocene Emplacement and Deformation of the Konga Shan Granite (Xianshui he Fault Zone, West Sichuan, China): Geodynamic Implications. *Earth and Planetary Science Letters*, 130(1/2/3/4): 201–216. https://doi.org/10.1016/0012-821x(94)00252-t

Schlagenhauf, A., Manighetti, I., Benedetti, L., et al., 2011. Earthquake Supercycles in Central Italy, Inferred from ^{36}Cl Exposure Dating. *Earth and Planetary Science Letters*, 307(3/4): 487–500. https://doi.org/10.1016/j.epsl.2011.05.022

Schwartz, D. P., Coppersmith, K. J., 1984. Fault Behavior and Characteristic Earthquakes: Examples from the Wasatch and San Andreas Fault Zones. *Journal of Geophysical Research*: *Solid Earth*, 89(B7): 5681–5698. https://doi.org/10.1029/jb089ib07p05681

Searle, M. P., Elliott, J. R., Phillips, R. J., et al., 2011. Crustal-Lithospheric Structure and Continental Extrusion of Tibet. *Journal of the Geological Society*, 168(3): 633–672. https://doi.org/10.1144/0016-76492010-139

Shan, B., Xiong, X., Wang, R. J., et al., 2013. Coulomb Stress Evolution along Xianshuihe-Xiaojiang Fault System since 1713 and Its Interaction with Wenchuan Earthquake, May 12, 2008. *Earth and Planetary Science Letters*, 377/378: 199–210. https://doi.org/10.1016/j.epsl.2013.06.044

Shao, Z. G., Xu, J., Ma, H. S., et al., 2016. Coulomb Stress Evolution over the Past 200 Years and Seismic Hazard along the Xianshuihe Fault Zone of Sichuan, China. *Tectonophysics*, 670: 48–65. https://doi.org/10.13039/501100001809

Shen, Z. K., Lü, J. N., Wang, M., et al., 2005. Contemporary Crustal Deformation around the Southeast Borderland of the Tibetan Plateau. *Journal of Geophysical Research*: *Solid Earth*, 110(B11): B11409. https://doi.org/10.1029/2004jb003421

Shi, F., He, H. L., Densmore, A. L., et al., 2016. Active Tectonics of the Ganzi-Yushu Fault in the Southeastern Tibetan Plateau. *Tectonophysics*, 676: 112–124. https://doi.org/10.1016/j.tecto.2016.03.036

Shimazaki, K., Nakata, T., 1980. Time-Predictable Recurrence Model for Large Earthquakes. *Geophysical Research Letters*, 7(4): 279–282. https://doi.org/10.1029/gl007i004p00279

Sieh, K., 1996. The Repetition of Large-Earthquake Ruptures. *Proceedings of the National Academy of Sciences*, 93(9): 3764–3771. https://doi.org/10.1073/pnas.93.9.3764

Sieh, K., Natawidjaja, D. H., Meltzner, A. J., et al., 2008. Earthquake Supercycles Inferred from Sea-Level Changes Recorded in the Corals of West Sumatra. *Science*, 322(5908): 1674–1678. https://doi.org/10.1126/science.1163589

Sieh, K., Stuiver, M., Brillinger, D., 1989. A more Precise Chronology of Earthquakes Produced by the San Andreas Fault in Southern California. *Journal of Geophysical Research*, 94(B1): 603–623. https://doi.org/10.1029/jb094ib01p00603

Stein, R. S., Barka, A. A., Dieterich, J. H., 1997. Progressive Failure on the North Anatolian Fault since 1939 by Earthquake Stress Triggering.

Geophysical Journal International, 128(3): 594–604. https://doi.org/10.1111/j.1365-246x.1997.tb05321.x

Stein, S., Geller, R. J., Liu, M., 2012. Why Earthquake Hazard Maps often Fail and what to do about it. *Tectonophysics*, 562/563: 1–25. https://doi.org/10.1016/j.tecto.2012.06.047

Tang, R., Wen, D., Deng, T., et al., 1976. A Preliminary Study on the Characteristics of the Ground Fracture during the Luhuo *M*=7.9 Earthquake, 1973 and the Origin of the Earthquake. *Acta Geophysica Sinica*, 19(1): 18–27 (in Chinese with English Abstract)

Thatcher, W., 1989. Earthquake Recurrence and Risk Assessment in Circum-Pacific Seismic Gaps. *Nature*, 341(6241): 432–434. https://doi.org/10.1038/341432a0

Toda, S., Lin, J., Meghraoui, M., et al., 2008. 12 May 2008 *M*=7.9 Wenchuan, China, Earthquake Calculated to Increase Failure Stress and Seismicity Rate on Three Major Fault Systems. *Geophysical Research Letters*, 35(17): L17305. https://doi.org/10.1029/2008gl034903

Toda, S., Stein, R. S., 2002. Response of the San Andreas Fault to the 1983 Coalinga-Nuñez Earthquakes: An Application of Interaction-Based Probabilities for Parkfield. *Journal of Geophysical Research*, 107(B6): ESE 6-1–ESE 6-16. https://doi.org/10.1029/2001jb000172

Toda, S., Stein, R. S., Richards-Dinger, K., et al., 2005. Forecasting the Evolution of Seismicity in Southern California: Animations Built on Earthquake Stress Transfer. *Journal of Geophysical Research*, 110(B5): B05S16. https://doi.org/10.1029/2004jb003415

Toda, S., Stein, R. S., Sevilgen, V., et al., 2011. Coulomb 3.3 Graphic-Rich Deformation and Stress-Change Software for Earthquake, Tectonic, and Volcano Research and Teaching—User Guide. U.S. Geological Survey Open-File Report 2011–106063. U.S. Geological Survey, [S.l.]

Wallace, R. E., 1970. Earthquake Recurrence Intervals on the San Andreas Fault. *Geological Society of America Bulletin*, 81(10): 2875–2890. https://doi.org/10.1130/0016-7606(1970)81[2875:eriots]2.0.co;2

Wang, C. Y., Han, W. B., Wu, J. P., et al., 2007. Crustal Structure beneath the Eastern Margin of the Tibetan Plateau and Its Tectonic Implications. *Journal of Geophysical Research*, 112(B7): 3672–3672. https://doi.org/10.1029/2005jb003873

Wang, C. Y., Lou, H., Wang, X. L., et al., 2009. Crustal Structure in Xiaojiang Fault Zone and Its Vicinity. *Earthquake Science*, 22(4): 347–356. https://doi.org/10.1007/s11589-009-0347-0

Wang, D., Mori, J., 2012. The 2010 Qinghai, China, Earthquake: A Moderate Earthquake with Supershear Rupture. *Bulletin of the Seismological Society of America*, 102(1): 301–308. https://doi.org/10.1785/0120110034

Wang, E., Burchfiel, B. C., 2000. Late Cenozoic to Holocene Deformation in Southwestern Sichuan and Adjacent Yunnan, China, and Its Role in Formation of the Southeastern Part of the Tibetan Plateau. *Geological Society of America Bulletin*, 112(3): 413–423. https://doi.org/10.1130/0016-7606(2000)112<413:lcthdi>2.0.co;2

Wang, E., Burchfiel, B. C., Royden, L. H., et al., 1998. Late Cenozoic Xianshuihe-Xiaojiang, Red River, and Dali Fault Systems of Southwestern Sichuan and Central Yunnan, China. *Special Paper of the Geological Society of America*, 327: 1–108. https://doi.org/10.1130/0-8137-2327-2.1

Wang, S. F., Fang, X. M., Zheng, D. W., et al., 2009. Initiation of Slip along the Xianshuihe Fault Zone, Eastern Tibet, Constrained by K/Ar and Fission-Track Ages. *International Geology Review*, 51(12): 1121–1131. https://doi.org/10.1080/00206810902945132

Wang, Y. Z., Wang, M., Shen, Z. K., et al., 2013. Inter-Seismic Deformation Field of the Ganzi-Yushu Fault before the 2010 M_w 6.9 Yushu Earthquake.

Tectonophysics, 584: 138–143. https://doi.org/10.1016/j.tecto.2012.03.026

Wells, D. L., Coppersmith, K. J., 1994. New Empirical Relationships among Magnitude, Rupture Length, Rupture Width, Rupture Area, and Surface Displacement. *Bulletin of the Seismological Society of America*, 84(4): 974–1002

Wen, X. Z., Ma, S. L., Xu, X. W., et al., 2008. Historical Pattern and Behavior of Earthquake Ruptures along the Eastern Boundary of the Sichuan-Yunnan Faulted-Block, Southwestern China. *Physics of the Earth and Planetary Interiors*, 168(1/2): 16–36. https://doi.org/10.1016/j.pepi.2008.04.013

Wen, X. Z., Xu, X. W., Zheng, R., et al., 2003. Average Slip-Rate and Recent Large Earthquake Ruptures along the Garzê-Yushu Fault. *Science in China Series D: Earth Sciences*, 46(2): 276–288

Wesnousky, S. G., 1994. The Gutenberg-Richter or Characteristic Earthquake Distribution, Which is it? *Bulletin of the Seismological Society of America*, 84(6): 1940–1959

Xu, L. L., Rondenay, S., van der Hilst, R. D., 2007. Structure of the Crust beneath the Southeastern Tibetan Plateau from Teleseismic Receiver Functions. *Physics of the Earth and Planetary Interiors*, 165(3/4): 176–193. https://doi.org/10.1016/j.pepi.2007.09.002

Yan, B., Lin, A. M., 2015. Systematic Deflection and Offset of the Yangtze River Drainage System along the Strike-Slip Ganzi-Yushu-Xianshuihe Fault Zone, Tibetan Plateau. *Journal of Geodynamics*, 87: 13–25. https://doi.org/10.13039/501100001700

Yan, B., Lin, A. M., 2017. Holocene Activity and Paleoseismicity of the Selaha Fault, Southeastern Segment of the Strike-Slip Xianshuihe Fault Zone, Tibetan Plateau. *Tectonophysics*, 694(2): 302–318. https://doi.org/10.13039/501100001700

Yan, J.-Q., Shi, Z.-L., Huan, W.-L., et al., 1980. The Characteristics of Fault Plane Solutions of Strong Aftershocks. *Acta Sedimentologica Sinica*, 2(4): 395–403 (in Chinese with English Abstract)

Yao, H. J., Beghein, C., van der Hilst, R. D., 2008. Surface Wave Array Tomography in SE Tibet from Ambient Seismic Noise and Two-Station Analysis-II. Crustal and Upper-Mantle Structure. *Geophysical Journal International*, 173(1): 205–219. https://doi.org/10.1111/j.1365-246x.2007.03696.x

Youngs, R. R., Coppersmith, K. J., 1985. Implications of Fault Slip Rates and Earthquake Recurrence Models to Probabilistic Seismic Hazard Estimates. *Bulletin of the Seismological Society of America*, 75(4): 939–964

Zhang, P. Z., 2013. A Review on Active Tectonics and Deep Crustal Processes of the Western Sichuan Region, Eastern Margin of the Tibetan Plateau. *Tectonophysics*, 584: 7–22. https://doi.org/10.1016/j.tecto.2012.02.021

Zhang, P. Z., Shen, Z. K., Wang, M., et al., 2004. Continuous Deformation of the Tibetan Plateau from Global Positioning System Data. *Geology*, 32(9): 809–812. https://doi.org/10.1130/g20554.1

Zhang, Z. J., Deng, Y. F., Teng, J. W., et al., 2011. An Overview of the Crustal Structure of the Tibetan Plateau after 35 Years of Deep Seismic Soundings. *Journal of Asian Earth Sciences*, 40(4): 977–989. https://doi.org/10.1016/j.jseaes.2010.03.010

Zhou, H., Liu, H.-L., Kanamori, H., 1983. Source Processes of Large Earthquakes along the Xianshuihe Fault in Southwestern China. *Bulletin of the Seismological Society of America*, 73(2): 537–551

Zhou, R. J., He, Y. L., Huang, Z. Z., et al., 2001a. The Slip Rate and Strong Earthquake Recurrence Interval on the Qianning-Kangding Segment of the Xianshuihe Fault Zone. *Acta Seismologica Sinica*, 14(3): 263–273. https://doi.org/10.1007/s11589-001-0004-8

Zhou, R. J., He, Y. L., Yang, T., et al., 2001b. Slip Rate and Strong Earthquake Rupture on the Moxi-Mianning Segment along the Xianshuihe-Anninghe Fault Zone. *Earthquake Research in China*, 17(3): 253–262 (in Chinese with English Abstract)

Zhou, R. J., Li, X. G., Huang, Z. Z., et al., 2003. Average Slip Rate of Daliang Mountain Fault Zone in Sichuan in Late Quaternary Period. *Journal of Seismological Research*, 26(2): 191–196 (in Chinese with English Abstract)

Zhou, R. J., Li, Y., Liang, M. J., et al., 2014. Determination of Mean Recurrence Interval of Large Earthquakes on the Garzê-Yushu Fault (Dengke Segment) on the Eastern Margin of the Qinghai-Tibetan Plateau. *Quaternary International*, 333: 179–187. https://doi.org/10.1016/j.quaint.2013.11.010

Zhou, R. J., Ma, S. H., Cai, C. X., 1996. Late Quaternary Active Features of the Ganzi-Yushu Fault Zone. *Earthquake Research in China*, 12(3): 250–260 (in Chinese with English Abstract)

Zhou, R. J., Wen, X. Z., Cai, C. X., et al., 1997. Recent Earthquakes and Assessment of Seismic Tendency on the Ganzi-Yushu Fault Zone. *Seismology and Geology*, 19(2): 115–124 (in Chinese with English Abstract)

Zhu, H., Wen, X. Z., 2010. Static Stress Triggering Effects Related with M_S 8.0 Wenchuan Earthquake. *Journal of Earth Science*, 21(1): 32–41. https://doi.org/10.1007/s12583-010-0001-8